PSFC/JA-20-117

Creation and Sustainment of Wide Pedestal Quiescent H-mode with Zero Net Neutral Beam Torque

K.H. Burrell[1], Xi Chen[1], C. Chrystal[1], B.A. Grierson[2], S.R. Haskey[2], T.H. Osborne[1], C. Paz-Soldan[1], T.M. Wilks[3]

[1] General Atomics, P.O. Box 85608, San Diego, California 92186-5608, USA
[2] Princeton Plasma Physics Laboratory PO Box 451, Princeton, NJ 08543-0451, USA
[3] MIT Plasma Science and Fusion Center NW16-258, 167 Albany St. Cambridge, MA 02139, USA

February 2020

Plasma Science and Fusion Center
Massachusetts Institute of Technology
Cambridge MA 02139 USA

This material is based upon work supported by the U.S. Department of Energy, Office of Science, Office of Fusion Energy Sciences, using the DIII-D National Fusion Facility, a DOE Office of Science user facility, under Award(s) DE-FC02-04ER54698, DE-AC02-09CH11466, and DE- SC0014264. Reproduction, translation, publication, use and disposal, in whole or in part, by or for the United States government is permitted.

Submitted to *Nuclear Fusion*

Creation and Sustainment of Wide Pedestal Quiescent H-mode with Zero Net Neutral Beam Torque

K.H. Burrell[1], Xi Chen[1], C. Chrystal[1], B.A. Grierson[2], S.R. Haskey[2], T.H. Osborne[1], C. Paz-Soldan[1], T.M. Wilks[3]

[1] General Atomics, P.O. Box 85608, San Diego, California 92186-5608, USA
[2] Princeton Plasma Physics Laboratory PO Box 451, Princeton, NJ 08543-0451, USA
[3] MIT Plasma Science and Fusion Center NW16-258, 167 Albany St. Cambridge, MA 02139, USA

ABSTRACT

Recent experiments in DIII-D have shown it is possible to create and sustain wide pedestal quiescent H-mode (QH-mode) plasmas with zero net torque from neutral beam injection (NBI) for the full discharge duration. Wide pedestal QH-mode has many of the features of the previously investigated QH-mode while having the advantage of increased edge pedestal pressure and energy confinement time. Both QH-mode variants operate without edge localized modes. Accordingly, these discharges demonstrate that significant input torque is not essential to the exploitation of wide pedestal QH-mode in future devices that are expected to have small or non-existent NBI torque. Developing operating conditions that allowed zero torque access to wide pedestal QH-mode required implementing several techniques to avoid locked modes including minimizing intrinsic error fields, avoiding large sawteeth, and driving toroidal rotation via neoclassical toroidal viscosity.

1. Introduction

Recent experiments in DIII-D have shown it is possible to create and sustain wide pedestal quiescent H-mode (QH-mode) with zero net torque from neutral beam injection (NBI) for the full discharge duration. Wide pedestal QH-mode [1-3] has many of the features of the previously investigated QH-mode [5,6] while having the advantage of increased edge pedestal pressure and energy confinement time. Although previous experiments demonstrated that wide pedestal QH-mode can exist with zero net NBI torque, the initial phase of those discharges operated with significant NBI torque in the direction opposite to the plasma current (counter-Ip) [1-3]. In the present experiments, as is illustrated in Fig. 1, we have shown that this initial counter-Ip torque can be removed while maintaining access to and operation of wide pedestal QH-mode. Accordingly, these discharges demonstrate that significant input torque is not essential to the exploitation of wide pedestal QH-mode in future devices with small or non-existent NBI torque.

In order to have sufficient energy confinement to reach burning plasma conditions, next step devices such as ITER [7] will operate in H-mode. This choice, however, comes at a significant potential cost because of the effects of edge localized modes (ELMs), which typically occur in the H-mode. Although ELM-induced particle transport has a beneficial effect in allowing density and impurity control, the ELM-induced, pulsed heat load to the divertor plates in ITER is calculated to be large enough to cause rapid erosion of those plates [7-9]. Accordingly, either significant ELM mitigation or, preferably, operation without ELMs is necessary. Operation should still maintain H-mode levels of energy confinement combined with adequate particle transport for helium ash removal and impurity control. Both wide pedestal and standard QH-mode operate without ELMs while exhibiting the H-mode edge pedestal and the associated H-mode level of energy confinement. Typical ITER H_{89} confinement enhancement factors [10] are at or above 2 and H_{98y2} is ≥1. In addition, even though they have no ELMs, the edge particle transport is rapid enough to provide particle exhaust in future devices [1,11,12].

QH-mode, a stationary H-mode without ELMs, was first discovered in DIII-D in 1999 [13-16] and was subsequently investigated on ASDEX-U [17-19], JET [19] and JT60-U [20, 21]. The initial discovery resulted from combining counter-I_p NBI with in-vessel cryopumping to operate at low density. Since the discovery of wide pedestal QH-mode in 2015 [1-3], the variant discovered in 1999 has been termed standard QH-mode. Experiments over roughly the next decade broadened the range of NBI torque in standard QH-mode to co-injection [5,22] and then to operation over a whole range of NBI torque [23-26], including operation with zero net NBI torque facilitated by using torque from neoclassical toroidal viscosity (NTV) [26] produced by nonresonant magnetic perturbations with toroidal mode number $n = 3$. The key to standard QH-mode operation with high edge rotational shear is the edge harmonic oscillation (EHO), which is a coherent, low *n* edge electromagnetic mode which provides the extra edge transport that allows a stationary transport equilibrium at edge conditions just below the stability boundary for ELMs. Typically, the EHO has multiple toroidal harmonics with the dominant toroidal mode number being $n = 1, 2$ or 3. Considerable work has been done which supports the paradigm [27, 28] that the EHO is a saturated kink-peeling mode destabilized by edge $\boldsymbol{E}\times\boldsymbol{B}$ shear [3, 29-31]. Interestingly, just as it does with microturbulence, $\boldsymbol{E}\times\boldsymbol{B}$ shear stabilizes high *n* peeling and ballooning modes but has the opposite effect on low *n* modes [27,28], which have no microturbulence analog. Detailed torque scans have shown that there is a critical $\boldsymbol{E}\times\boldsymbol{B}$ shear above which the EHO can exist [3,31].

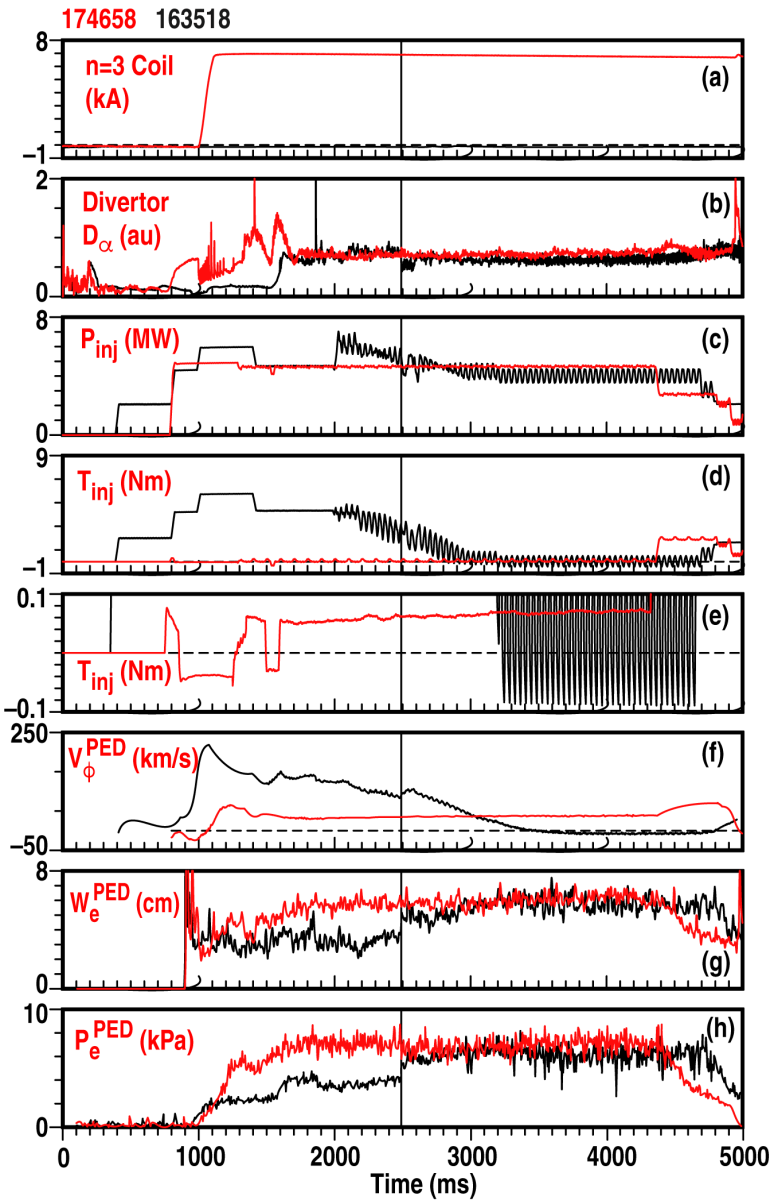

Figure 1. Time history of wide pedestal QH-Mode with net zero NBI torque throughout (red, shot 174658) compared with a shot using previous high counter NBI torque startup scenario (black, shot 163518). (a) Current in coil producing the non-resonant, $n = 3$ magnetic field; (b) Divertor D_α intensity showing no ELMs throughout the QH-mode phase of each shot; (c) Injected NBI power; (d) and (e) NBI torque input with two different vertical scales so that low input torque on red shot can be resolved; (f) pedestal toroidal rotation speed of the fully stripped carbon impurity in the plasmas; (g) width of edge electron pressure profile; (h) pedestal electron pressure. The sign convention for (d), (e) and (f) has positive values in the counter-I_p direction. Note that the width and pressure shown in (g) and (h) for the black shot rise to match that of the red around 2500 ms when the wide pedestal forms in the black shot. As can be seen in (e), the net NBI torque in shot 174658 is not exactly zero but ranges from +0.06 (counter-I_p) to -0.04 (co-I_p) Nm. These values are much smaller than the 6 Nm in the startup phase of shot 163518. Basic plasma conditions are 1.1 MA plasma current, 2.05 T on-axis toroidal field and 3.6 × 10^{19} m^{-3} line averaged density in the stationary phase of the discharges. The increase in the D_α intensity around 1550 ms in the black curve in (b) is due to changing the plasma shape from upper single null to double null. The vertical black line marks the time of the transition to wide pedestal QH-mode for the black curves.

Wide pedestal QH-mode was discovered in high triangularity, double null discharges during experiments where the NBI torque was ramped down [1-3]. As is illustrated in the black curves in Fig. 1, electron pedestal height and width rapidly increase at the transition from standard to wide pedestal QH-mode. The electron pedestal pressure increases on average by about 60%, pedestal width increases about 50% and global energy confinement increases about 40%; these increases are relative to the conditions in the preceding standard QH phase. The improved pedestal is achieved with reactor-relevant plasma parameters, normalized beta in the range $\beta_N = 1.5 - 2.3$, ITER 98y2 confinement enhancement factor $H_{98y2} = 1.2 - 1.6$, and pedestal collisionality $\nu_{*e}^{PED} = 0.3 - 0.4$. The bifurcation is associated with bimodal changes in the structure of the edge radial electric field well, an increase in the edge density fluctuations and a change in the magnetic fluctuations from the coherent EHO to more broadband MHD, as is shown in Fig. 2(b). In addition, unlike the limit cycle oscillations seen before some L to H transitions, which terminate at the transition [32], wide pedestal QH-mode exhibits a continuing limit cycle oscillation which may contribute to the edge transport [33,34]. Wide pedestal QH-mode has demonstrated stationary operation at zero net NBI torque and does not require NTV torque from nonaxisymmetric magnetic fields although it is compatible with it. The increased pedestal pressures are consistent with the peeling-ballooning stability embodied in the ELITE code [28]; the wide pedestal cases are somewhat further from the peeling boundary than the standard QH-mode; the increased pedestal width allows increased pedestal pressure while the edge plasma remains stable to peeling-ballooning modes [1-3].

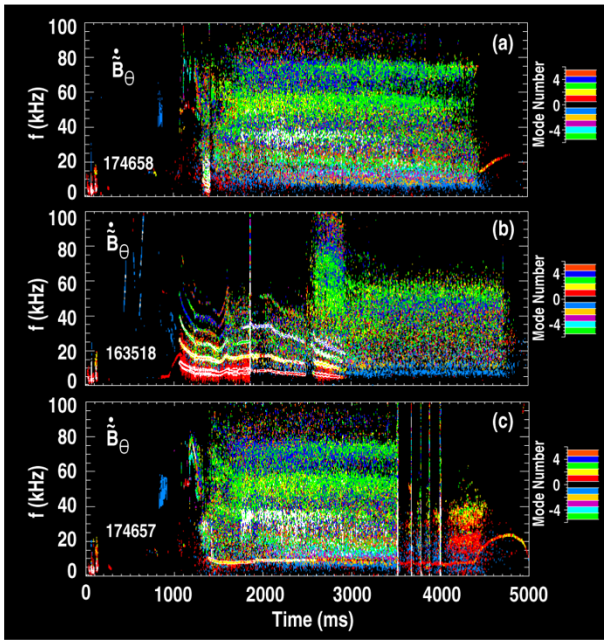

Figure 2. Spectrograms of magnetic probe signals as a function of time for three wide pedestal QH-mode shots. The top two are the same shots as in Fig. 1: (a) 174658 (red data in Fig. 1), (b) 163518 (black data in Fig 1) while (c) is another shot with net zero NBI torque throughout. Compare the coherent EHO in 163518 from 1000 to 3000 ms during the higher torque phase with the broadband MHD later in 163518 and throughout 174658. The wide pedestal transition in 163518 occurs about 2500 ms where there is a gap in the coherent EHO. The coherent EHO is present in 163518 during a portion of the wide pedestal phase. There is a very short coherent EHO phase in 174658 from 1300 to 1400 ms. In (c), there was a preprogramed shape change to lower single null discharge at 3500 ms which is associated with the transient return of ELMs. Note the $n = 2$ core tearing mode at about 9 kHz in (c). The color bars indicate the toroidal mode numbers.

2. Creation of Wide Pedestal QH-mode with Net Zero NBI Torque

After the demonstration of sustainment of standard QH-mode with zero net NBI torque [23,24], several attempts were made to create QH-mode with zero NBI torque; until the present experiment, all were unsuccessful owing to the occurrence of locked modes [35-37]. Once a locked mode occurs, plasma confinement is significantly degraded and, often, disruption results. Accordingly, a key part of the present experiment was developing and utilizing techniques to avoid locked modes.

Tokamak plasmas are more subject to locked modes when the initial plasma toroidal rotation is small, which is the case without additional torque input. In addition, locked modes occur more readily in plasmas with non-axisymmetric, low n magnetic perturbations, often due to intrinsic error fields related to small construction errors [35-37]. Furthermore, pulsive MHD events such as sawteeth or ELMs can trigger locked modes. Finally, mode locking is more frequent when coherent, low n MHD modes are present in the plasma. These can either be core tearing modes or the EHO itself, especially when the $n = 1$ component is dominant. We took several steps to eliminate or minimize all of these effects.

First, in addition to NBI torque, plasma rotation can also be driven by the NTV torque due to externally imposed, static nonaxisymmetric fields [23-26]. Accordingly, the technique we used to produce shots like 174658 in Fig. 1 was to utilize the NTV torque from $n = 3$ fields to produce counter-Ip plasma rotation even with very small NBI torque. The NTV torque was produced using the so-called C-coil, which is a six-segment coil mounted outside the toroidal coil on DIII-D [38,39]. The NTV torque depends on the edge ion temperature gradient and, hence, is much smaller in L-mode. We found that, as is shown in Fig. 1(a), turning the $n = 3$ coil on at the time of the L to H transition drove the plasma rotation in the counter-Ip direction, as can be seen in Fig. 1(f) at about 1000 ms. Comparing the rotation profiles in Fig. 3 demonstrates the significant effect of the NTV torque on the toroidal rotation under conditions of essentially zero net NBI torque. Indeed, the effect of the NTV torque is strong enough that, as shown in Fig. 2(c), even shots with a core tearing mode run stably because the plasma rotation is rapid enough to prevent mode locking.

Second, the intrinsic error fields in DIII-D were minimized by using additional non-axisymmetric fields from the DIII-D I-coil, which is a 12-segment coil mounted inside the vacuum vessel with six segments above and six below the vessel midplane [39]. Currents in these segments were adjusted to minimize the error fields from the other DIII-D coils using algorithms developed from previous error field investigations [39]. These correction fields are primarily $n = 1$. In 2017, a wiring error was found and fixed in the C-coil which had produced an unwanted $n = 1$ component even when the coil was nominally wired for $n = 3$. This may have adversely affected our previous attempts at creation of QH-mode with net zero NBI torque.

Third, by starting the NBI early in the shot right at the time that the plasma current reaches flattop, the current profile is broad enough that there are no sawteeth which could trigger locked modes. The on-axis safety factor $q(0)$ remains high enough that sawteeth never occur in these shots. We speculate that the increased edge bootstrap current from the increased pedestal pressure allows a broad current profile with $q(0) > 1$. In addition, operation without ELMs prevents ELM-triggered locked modes. Finally, the lack of the coherent EHO during the initial 500 ms of the NBI pulse also removes the $n = 1$ component as a possible source of mode locking.

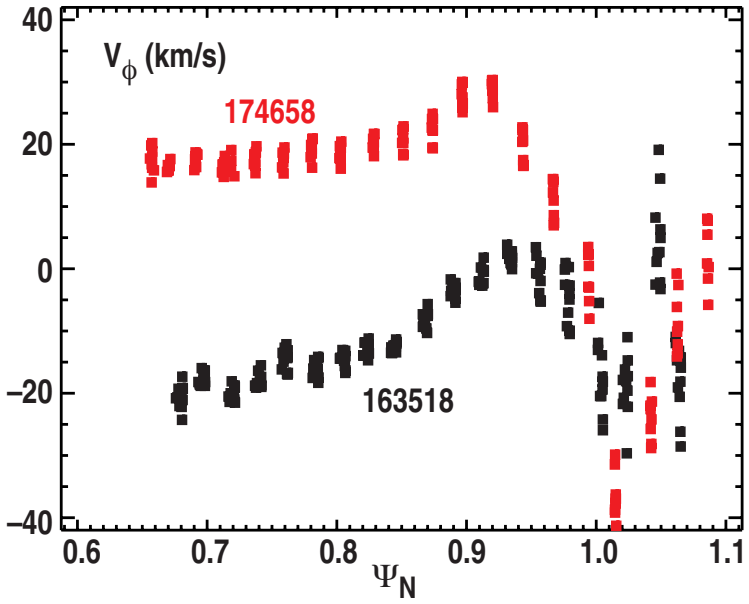

Figure 3 Toroidal rotation speed for fully stripped carbon ions determined from charge exchange spectroscopy for two shots, one with additional NTV torque (red) and the other without (black). The comparison is made at 4000 ms into the two discharges (see Fig. 1). The x-axis is the radial coordinate based on the normalized poloidal magnetic flux. The sign convention for the plot is that positive values are in the counter-I_p direction.

The pedestal width evolution in Fig. 1(g) is different for the two shots shown. There is no obvious bifurcation in the shot with net zero NBI torque throughout; instead, the width gradually evolves over several hundred milliseconds. This raises the question of whether the shots with net zero NBI torque startup are truly wide pedestal QH-modes. As one demonstration of this, Fig. 2 shows that the shots with zero torque startup have the same broadband MHD as the shot with the torque rampdown. The broadband MHD is a characteristic signature of wide pedestal QH-mode. During the stationary phase of most wide pedestal QH-modes, the coherent EHO is absent although, as seen in Fig. 2(b), the coherent EHO can sometimes persist during the initial portion of the wide pedestal shots formed with torque rampdown.

A second, clearer demonstration that the zero torque startup shots are wide pedestal is given in Fig. 4. Here, we compare the measured electron pressure pedestal width with the prediction of the EPED model [40] in a net zero NBI torque shot and a standard QH-mode shot with strong, counter-I_p NBI torque. The defining characteristic of the wide pedestal QH-mode is that the pressure profile pedestal width significantly exceeds that predicted by EPED [1-3]. As can be seen in Fig. 4(a), the measured pedestal width does significantly exceed the EPED prediction in the shot with net zero NBI torque while the measured width in Fig. 4(b) matches the EPED prediction quite well until a shape change and torque stepdown after 4000 ms cause a transition to the wide pedestal state. As can be seen in Fig. 5, the shape of the standard QH-mode plasma shown in Fig. 4 before the shape change is a slightly upper single null while the net zero NBI torque shot is a slightly lower single null. In general, wide pedestal QH-mode is easier to access when the ion $\boldsymbol{B} \times \nabla B$ drift is towards the divertor X-point [41]; that drift is downwards in these shots.

The most complete demonstration of the wide pedestal character of the shots with net zero torque startup can be seen in Fig. 6. It is clear that the pedestal is wider in both the electron and ion transport channels. In addition, the region over which the radial electric field E_r has a significant shear is wider in the shot with net zero NBI torque. This can be seen both in the E_r profile in Fig.

6(e) and in the profile of the Hahm-Burrell $\boldsymbol{E}\times\boldsymbol{B}$ shearing rate [42] in Fig. 6(f). Unlike previous comparisons of wide pedestal and standard QH-mode [1-3] which were done at constant input power, the results in Figs. 4-6 are shown at constant $\beta_N = 1.7$, which means significantly different input powers and, hence, different energy confinement times, as indicated in the caption in Fig. 6. This increase of energy confinement time with decreasing input torque has also been seen in standard QH-mode [23,24].

Comparing the E_r and $\boldsymbol{E}\times\boldsymbol{B}$ shearing rate profiles at constant β_N rather than at constant NBI power reveals some striking differences in the results. At constant power [1-3], the minimum in the E_r well is deeper in the standard QH-mode case and the $\boldsymbol{E}\times\boldsymbol{B}$ shearing rate around $\psi_N = 0.93$ is higher in the standard QH-mode. However, in the case in Fig. 6, the minimum in the E_r well and the $\boldsymbol{E}\times\boldsymbol{B}$ shearing rate around $\psi_N = 0.93$ are about the same for the two shots. Both at constant power and at constant β_N, the $\boldsymbol{E}\times\boldsymbol{B}$ shearing rate from $\psi_N \sim 0.8$ to $\psi_N \sim 0.9$ is higher in the wide pedestal case. It is this latter difference that is a key feature of the wide pedestal state. Previous work suggests that this latter difference is the cause of the increase in energy confinement time [1-3].

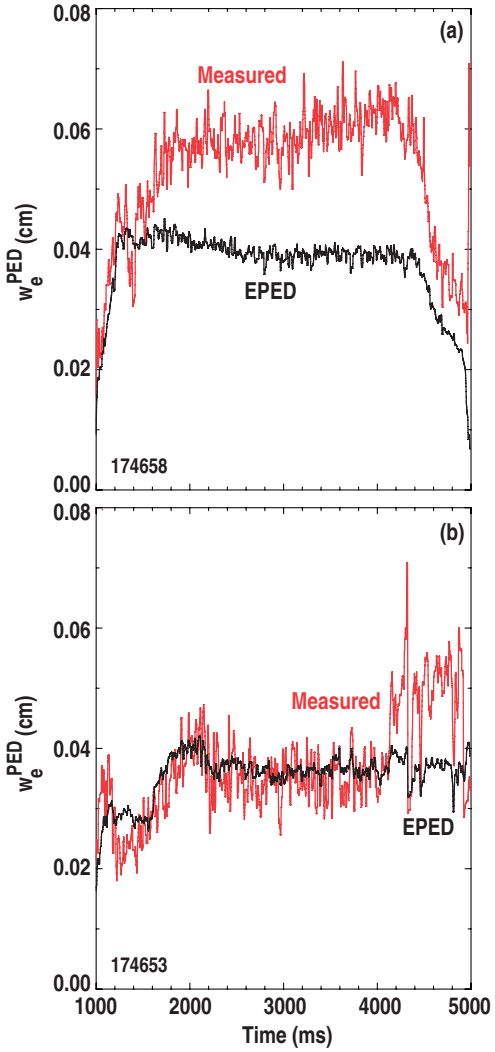

Figure 4. Width of the electron pressure pedestal as a function of time comparing the measured width with the predictions of the EPED model. (a) Comparison for the zero net NBI torque shot 174658, (b) comparison for a shot, 174653, which is standard QH-mode with 5 Nm counter-I_p NBI torque until 4000 ms.

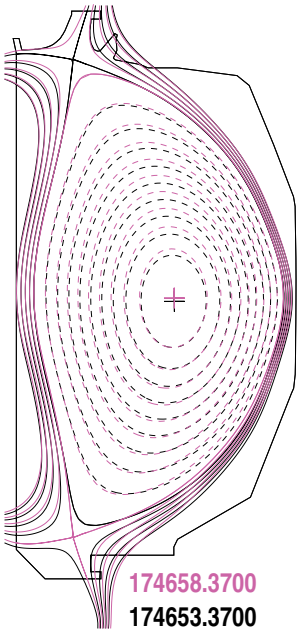

Figure 5. Comparison of plasma shapes for a wide pedestal QH-mode, shot 174658 (red) and a standard QH-mode, shot 174653 (black). The wide pedestal shot is slightly lower single null with Drsep = - 4 mm while the standard QH-mode is slightly upper single null with Drsep = + 1 mm. Drsep is the distance between the two magnetic separatrices measured at the outboard midplane of the plasma.

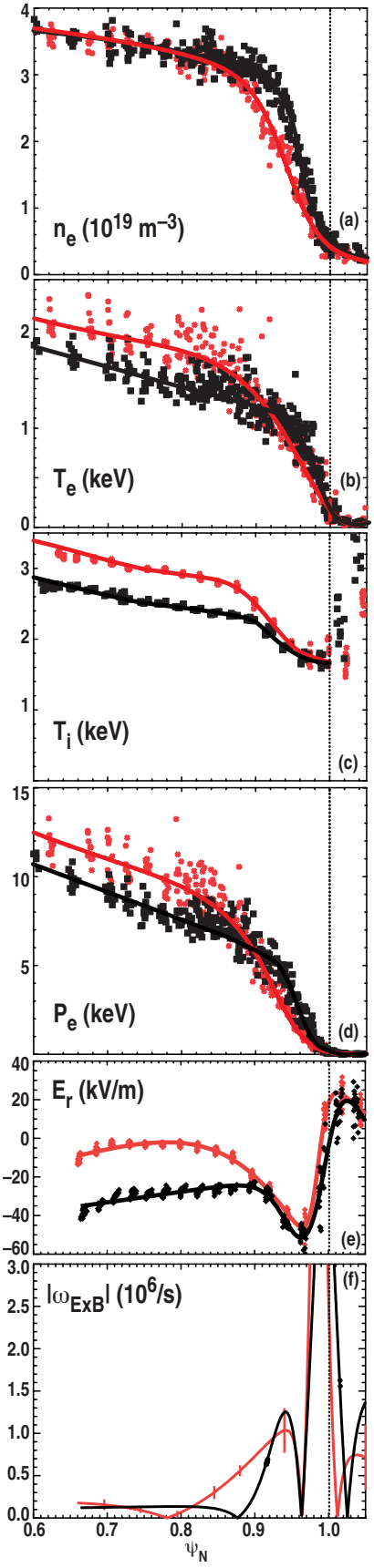

Figure 6. Radial profiles at 3700 ms of the two QH-mode shots shown in Figs. 4 and 5, shot 174658 (red) is a wide pedestal QH-mode and 174653 (black) is a standard QH-mode. Profiles are averaged over a 100 ms interval centered on 3700 ms. (a) Electron density profile, (b) electron temperature profile, (c) ion temperature profile, (d) electron pressure profile, (e) profile of the radial electric field, and (f) profile of the absolute value of the $\boldsymbol{E}\times\boldsymbol{B}$ *shear. Error bars on the* $\boldsymbol{E}\times\boldsymbol{B}$ *shear are the population standard deviation computed from the 100 ms long time series. These two shots make a particularly nice comparison since they both have* $\beta_N = 1.7$*, plasma current 1.1 MA, toroidal field 2.05 T,* $q_{95} = 5.5$*, and have the same pedestal and line averaged densities. In order to achieve the same* β_N*, the NBI power increased from 4.6 MW in the wide pedestal case to 7.5 MW in the standard QH-mode while the energy confinement time decreased from 150 ms to 93 ms (ratio 1.6) and the ITER98y2 factor decreased from 1.3 to 0.91 (ratio 1.4). The x-axis is the radial coordinate based on the normalized poloidal magnetic flux.*

3. Issues for future work

The present results are an important achievement since they demonstrate that wide pedestal QH-mode can be created and sustained at the low NBI torque levels anticipated in future devices. However, they are only one step along the road to that goal.

The criterion used in this paper for low NBI torque is based on the torque input from the neutral particles injected into the plasma. Experimentally, creating and sustaining plasmas with zero net NBI torque has always been the most difficult operating condition. However, because of fast ion orbit effects and edge fast ion loss, zero net NBI torque does not mean that the torque density coupled to the thermal plasma from the fast ions is zero at each point in the plasma for plasmas in DIII-D. As can be seen in Fig. 7, the volume integrated torque density coupled to the thermal plasma for the zero NBI torque shot is actually a bit co-I_p in the bulk but becomes counter-I_p near the edge. This leads to the question whether these fast ion effects, which will be different in larger devices, might affect the use of wide pedestal QH-mode in those devices. However, as can also be seen in Fig. 7, wide pedestal QH-mode can be sustained with a range of torque profiles, suggesting that the detailed volume integrated torque profile is not relevant. (The results in Fig. 7 were calculated using the NUBEAM code [43] using the measured experimental plasma profiles as input.) Additional evidence that the details of the torque input is not relevant can be seen in the even wider range of NBI torque inputs in wide pedestal QH-mode discussed in [41].

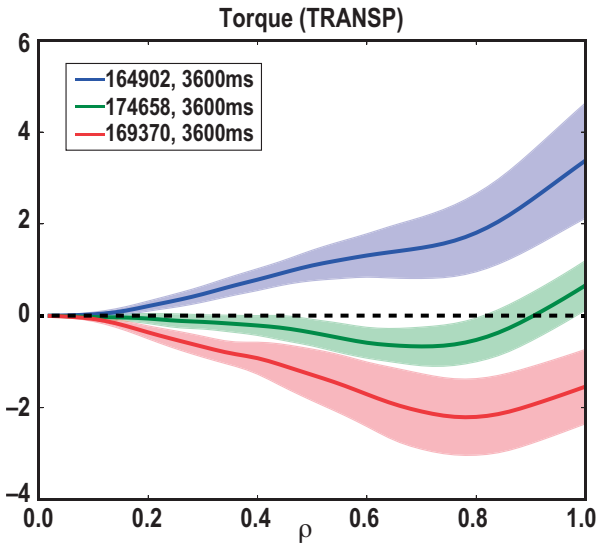

Figure 7. Volume integral of the torque density coupled to the thermal plasma by the fast ions for three wide pedestal QH-mode plasmas. The integral is from the magnetic axis to a given minor radius. The torque density is calculated using the NUBEAM code [43] and the shaded error bands are due to statistics from the Monte Carlo calculation. The sign convention for the plot has positive values in the counter-Ip direction. The net neutral torque from the beams is -1.9 Nm for shot 169370 (co-Ip), -0.04 Nm for 174658 and + 2.0 Nm (counter-Ip) for 164902. The x-axis is the radial coordinate proportional to the square root of the toroidal magnetic flux, normalized to unity at the separatrix.

For confident extrapolation of present-day wide pedestal QH-mode results to future devices, we need a predictive understanding of how the H-mode edge evolves into the wide pedestal state under low torque operation in highly shaped plasmas. A key part of this predictive understanding requires understanding the edge plasma rotation, including the effects of NBI torque, NTV torque and the self-generated intrinsic torque [44]. This work also needs to consider that, as can be seen in Fig. 8, the measured toroidal rotation is significantly different for the deuterons and the fully stripped carbon ions. (Details of the measurement techniques used for the data in Fig. 8 can be

found in [45,46].) The carbon ion measurement is the one usually used for toroidal rotation measurements in most tokamaks. However, in regions of steep pressure gradients, such as the edge pedestal, the radial force balance equation

$$E_r = \frac{1}{n_i Z_i e} \nabla p_i - v_{i\phi} B_\theta + v_{i\theta} B_\phi \quad (1)$$

indicates that the different ion species must have different rotation. In Eq. (1), n_i is the density of a given species, $Z_i e$ is the charge of that species, $p_i = n_i T_i$ is the pressure, T_i is the temperature, $v_{i\phi}$ is the toroidal rotation speed, $v_{i\theta}$ is the poloidal rotation speed, B_ϕ is the toroidal component of the magnetic field and B_θ is the poloidal component of that field. The data in Fig. 8 for fully stripped carbon ions and deuterons is consistent with the expectation that the differences in the rotation of these ions are greatest where the pressure gradient is largest.

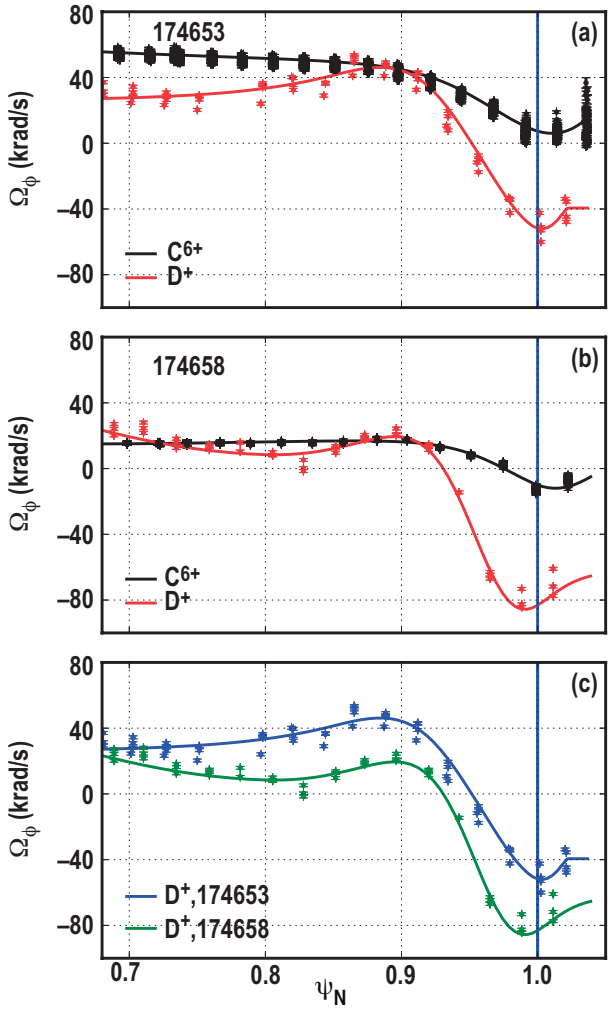

Figure 8. Radial profile of toroidal angular rotation speed (v_ϕ/R) measured using charge exchange spectroscopy at 3700 ms in the two QH-mode shots shown in Figs 4, 5 and 6. (a) Comparison of rotation for fully stripped carbon ions and deuterons for the standard QH-mode shot, 174653; (b) Comparison of rotation for fully stripped carbon ions and deuterons for the wide pedestal QH-mode shot, 174658; and (c) Comparison of deuteron rotation profiles for the two shots. The x-axis is the radial coordinate based on the normalized poloidal magnetic flux.

4. Conclusion

Recent experiments in DIII-D have demonstrated creation and sustainment of wide pedestal QH-mode with zero net torque from NBI. These results show it is possible to overcome the difficulties associated with zero NBI torque operation and provide an existence proof for operation without ELMs at NBI torque levels relevant for future devices. Developing operating conditions that allowed zero torque startup required implementing several techniques to avoid locked modes.

Wide pedestal QH-mode has many of the features of the previously investigated QH-mode while having the advantage of increased edge pedestal pressure and energy confinement time. Although these results are a significant step along the road to ELM-free operation in future devices, considerable work still remains to do to develop the predictive understanding of edge plasma rotation required for confident extrapolation of present results to those devices.

This material is based upon work supported by the U.S. Department of Energy, Office of Science, Office of Fusion Energy Sciences, using the DIII-D National Fusion Facility, a DOE Office of Science user facility, under Award(s) DE-FC02-04ER54698, DE-AC02-09CH11466, and DE-SC0014264.

REFERENCES

[1] K. H. Burrell, K. Barada, X. Chen, A. M. Garofalo, R. J. Groebner, C. M. Muscatello, T. H. Osborne, C. C. Petty, T. L. Rhodes, P. B. Snyder, W. M. Solomon, Z. Yan, and L. Zeng, Phys. Plasmas **23**, 056103 (2016).

[2] Xi Chen, K.H. Burrell, T.H. Osborne, W.M. Solomon, K. Barada, A.M. Garofalo, R.J. Groebner, N.C. Luhmann, G.R. McKee, C.M. Muscatello, M. Ono, C.C. Petty, M. Porkolab, T.L. Rhodes, J.C. Rost, P.B. Snyder, G.M. Staebler, B.J. Tobias, Z. Yan and the DIII-D Team, Nucl. Fusion **57**, 022007 (2017).

[3] Xi Chen, K.H. Burrell, T.H. Osborne, K. Barada, N.M. Ferraro, A.M. Garofalo, R.J. Groebner, G.R. McKee, C.C. Petty, M. Porkolab, T.L. Rhodes, J.C. Rost, P.B. Snyder, W.M. Solomon, Z. Yan, Nuclear Fusion **57**, 086008 (2017).

[5] K.H. Burrell, W.P. West, E.J. Doyle, M.E. Austin, T.A. Casper, P. Gohil, C.M. Greenfield, R.J. Groebner, A.W. Hyatt, R.J. Jayakumar, D.H. Kaplan, L.L. Lao, A.W. Leonard, M.A. Makowski, G.R. McKee, T.H. Osborne, P.B. Snyder, W.M. Solomon, D.M. Thomas, T.L. Rhodes, E.J. Strait, M.R. Wade, G. Wang, and L. Zeng, Phys. Plasmas **12**, 056121 (2005).

[6] K.H. Burrell, T.H. Osborne, P.B. Snyder, W.P. West, M.E. Fenstermacher, R.J. Groebner, P. Gohil, A.W. Leonard, and W.M. Solomon, Nucl. Fusion **49**, 085024 (2009).

[7] A. Loarte, G. Huijsmans, S. Futatani, L.R. Baylor, T.E. Evans, D. M. Orlov, O. Schmitz, M. Becoulet, P. Cahyna, Y. Gribov, A.Kavin, A. Sashala Naik, D.J. Campbell,T. Casper, E. Daly, H. Frerichs, A. Kischner, R. Laengner,S. Lisgo, R.A. Pitts, G. Saibene and A. Wingen, Nucl. Fusion **54**, 033007 (2014).

[8] A. Loarte, B. Lipschultz, A.S. Kukushkin, G.F. Matthews, P.C. Stangeby, N. Asakura, G.F. Counsell, G. Federici, A. Kallenbach, K. Krieger, M.A. Mahdavi, V. Philipps, D. Reiter, J. Roth, J. Strachan, D. Whyte, R. Doerner, T. Eich, W. Fundamenski, A. Herrmann, M. Fenstermacher, P. Ghendrih, M. Groth, A. Kirschner, S. Konoshima, B. LaBombard, P. Lang, A.W. Leonard, P. Monier-Garbet, R. Neu, H. Pacher, B. Pegourie, R.A. Pitts, S. Takamura, J. Terry, E. Tsitrone and the ITPA Scrape-off Layer and Divertor Physics Topical Group, Nucl. Fusion 47, S203 (2007).

[9] P.T. Lang, A. Loarte, G. Saibene, L.R. Baylor, M. Becoulet, M. Cavinato,S. Clement-Lorenzo, E. Daly, T.E. Evans, M.E. Fenstermacher, Y. Gribov, L.D. Horton, C. Lowry, Y. Martin, O. Neubauer, N. Oyama, M.J. Schaffer, D. Stork, W. Suttrop, P. Thomas, M.Tran, H.R. Wilson, A.Kavin and O. Schmitz, Nucl. Fusion **53**, 043004 (2013).

[10] ITER Physics Basis Document, Nucl. Fusion **39**, 2137 (1999).

[11] B. A. Grierson, K. H. Burrell,R. M. Nazikian, W. M. Solomon, A. M. Garofalo, E. A. Belli, G. M. Staebler, M. E. Fenstermacher, G. R. McKee, T. E. Evans, D. M. Orlov, S. P. Smith, C. Chrobak, C. Chrystal, and DIII-D Team, Phys. Plasmas **22**, 055901 (2015).

[12] B.A. Grierson, K.H. Burrell, A.M. Garofalo, W.M. Solomon, A. Diallo and M. O'Mullane, Nucl. Fusion **54**, 114011 (2014).

[13] K. H. Burrell, C.M. Greenfield, C. Rost, M.R. Wade, and W.P. West, Bull. Am. Phys. Soc. **44**, 127 (1999).

[14] K.H. Burrell, M.E. Austin, D.P. Brennan, J.C. DeBoo, E.J. Doyle, C. Fenzi, C. Fuchs, P. Gohil, C.M. Greenfield, R.J. Groebner, L.L. Lao, T.C. Luce, M.A. Makowski, G.R. McKee, R.A. Moyer, C.C. Petty, M. Porkolab, C.L. Rettig, T.L. Rhodes, J.C. Rost, B.W. Stallard, E.J. Strait, E.J. Synakowski, M.R. Wade, J.G. Watkins, and W.P. West, Phys. Plasmas **8**, 2153 (2001).

[15] C.M. Greenfield, K.H. Burrell, J.C. DeBoo, E.J. Doyle, B.W. Stallard, E.J. Synakowski, C. Fenzi, P. Gohil, R.J. Groebner, L.L. Lao, M.A. Makowski, G.R. McKee, R.A. Moyer, C.L. Rettig, T.L. Rhodes, R.I. Pinsker, G.M. Staebler, and W.P. West, Phys. Rev. Lett. **86**, 4544 (2001).

[16] E.J. Doyle, L.R. Baylor, K.H. Burrell, T.A. Casper, J.C. DeBoo, D.R. Ernst, A.M. Garofalo, P. Gohil, C.M. Greenfield, R.J. Groebner, A.W. Hyatt, G.L. Jackson, T.C. Jernigan, J.E. Kinsey, L.L. Lao, C.J. Lasnier, J.-N. Leboeuf, M. Makowski, G.R. McKee, R.A. Moyer, M. Murakami, T.H. Osborne, W.A. Peebles, M. Porkolab, G.D. Porter, T.L. Rhodes, J.C. Rost, D. Rudakov, G.M. Staebler, B.W. Stallard, E.J. Strait, R.D. Sydora, E.J. Synakowski, M.R. Wade, G. Wang, J.G. Watkins, W.P. West and L. Zeng, Plasma Phys. Control. Fusion **43**, A95 (2001).

[17] W. Suttrop, M. Maraschek, G.D. Conway, H.-U. Fahrbach, G. Haas, L.D. Horton, T. Kurki-Suonio, C.J. Lasnier, A.W. Leonard, C.F. Maggi, H. Meister, A. Mueck, R. Neu, I. Nunes, Th. Puetterich, M. Reich, A.C.C. Sips, and the ASDEX Upgrade Team, Plasma Phys. Controlled Fusion 45, 1399 (2003).

[18] W. Suttrop, M. Maraschek, G.D. Conway,H.-U. Fahrback, G. Haas, L.D. Horton, T. Kurki-Suonio, C.F. Maggi, H.Meister, A. Mück, R. Neu, I. Nunes, Th. Pütterich, M. Reich, and A.C.C.Sips and the ASDEX-Upgrade team, Plasma Phys. Controlled Fusion **46**, A151 (2004)

[19] W. Suttrop, V. Hynoenen, T. Kurki-Suonio, P.T. Lang, M. Maraschek, R. Neu, A. Staebler, G. D. Conway, S. Hacquin, M. Kempenaars, P.J. Lomas, M.F.F. Nave, R.A. Pitts, K.-D. Zastrow, the ASDEX Upgrade Team, and Contributors to the JET-EFDA Workprogramme, Nucl. Fusion **45**, 721 (2005).

[20] Y. Sakamoto, H. Shirai, T. Fujita, S. Ide, T. Takizuka, N. Oyama, and Y. Kamada, Plasma Phys. Controlled Fusion **46**, A299 (2004).

[21] N. Oyama, Y. Sakamoto, A. Isayama, M. Takechi, P. Gohil, L.L. Lao, P.B. Snyder, T. Fujita, S. Ide, Y. Kamada, Y. Miura, T. Oikawa, T. Suzuki, H. Takenaga, K. Toi, and the JT-60 Team, Nucl. Fusion **45**, 871 (2005).

[22] K. H. Burrell, T. H. Osborne, P. B. Snyder, W. P. West, M. E. Fenstermacher, R. J. Groebner, P. Gohil, A. W. Leonard, and W. M. Solomon, Phys. Rev. Lett. 102, 155003 (2009).

[23] A.M. Garofalo, W.M. Solomon, J.-K. Park, K.H. Burrell, J.C. DeBoo, M.J. Lanctot, G.R. McKee, H. Reimerdes, L. Schmitz, M.J. Schaffer and P.B. Snyder, Nucl. Fusion 51, 083018 (2011).

[24] K.H. Burrell, A.M Garofalo, W.M. Solomon, M.E. Fenstermacher, T.H. Osborne, J.-K. Park, M.J. Schaffer, and P.B. Snyder, Phys. Plasmas **19**, 056117 (2012).

[25] K.H. Burrell, A.M. Garofalo, W.M. Solomon, M.E. Fenstermacher, D.M. Orlov, T.H. Osborne, J.-K. Park and P.B. Snyder, Nucl. Fusion **53**, 073038 (2013).

[26] A.M.Garofalo, K.H.Burrell, D.Eldon, B.A.Grierson, J.M.Hanson, C.Holland, G.T.A.Huijsmans, F.Liu, A.Loarte, O.Meneghini, T.H.Osborne, C.Paz-Soldan, S.P.Smith, P.B. Snyder, W.M.Solomon, A.D.Turnbull, and L.Zeng, Phys. Plasmas **22**, 056116 (2015).

[27] P.B. Snyder, T.H. Osborne, K.H. Burrell, R.J. Groebner, A.W. Leonard, R. Nazikian, D.M. Orlov, O. Schmitz, M.R. Wade, and H. R. Wilson, Phys. Plasmas **19**, 056115 (2012).

[28] P. B. Snyder, K. H. Burrell, H. R. Wilson, M. S. Chu, M. E. Fenstermacher, A. W. Leonard, R. A. Moyer, T. H. Osborne, M. Umansky, W. P. West, and X. Q. Xu, Nucl. Fusion **47**, 961 (2007).

[29] T.H. Osborne, P.B. Snyder, K.H. Burrell, T.E. Evans, M.E. Fenstermacher, A.W. Leonard, R.A. Moyer, M.J. Schaffer and W.P. West, J. Phys.: Conf. Ser. **123**, 012014 (2008).

[30] Xi Chen, K.H. Burrell, N.M. Ferraro, T.H. Osborne, M.E. Austin, A.M. Garofalo, R.J. Groebner, G.J. Kramer, N.C. Luhmann Jr, G.R. McKee, C.M. Muscatello, R. Nazikian, X. Ren, P.B. Snyder, W.M. Solomon, B.J. Tobias and Z. Yan, Nucl. Fusion **56,** 076011 (2016).

[31] T.M. Wilks, A.M. Garofalo, P.H. Diamond, Z.B. Guo, J.W. Hughes, K.H. Burrell and Xi Chen, Nucl. Fusion **58**, 112002 (2018).

[32] L. Schmitz, Nucl. Fusion **57**, 025003 (2017).

[33] K. Barada, T. L. Rhodes, K. H. Burrell, L. Zeng, L. Bardóczi, Xi Chen, C. M. Muscatello, and W. A. Peebles, Phys. Rev. Lett. 120, 135002 (2018).

[34] K. Barada, T. L. Rhodes, K. H. Burrell, L. Zeng, Xi Chen, M. Austin, L. Bardóczi, C.M. Muscatello, and W. A. Peebles, Phys. Plasmas **26**, (in press).

[35] R. J. La Haye, R. Fitzpatrick, T. C. Hender, A. W. Morris, J. T. Scoville, and T. N. Todd, Phys. Fluids **B 4**, 2098 (1992).

[36] E. Lazzaro, R. J. Buttery, T. C. Hender, P. Zanca, R. Fitzpatrick, M. Bigi, T. Bolzonella, R. Coelho, M. DeBenedetti, S. Nowak, O. Sauter, M. Stamp, and Contributors to the EFDA-JET work programme
Phys. Plasmas 9, 3906 (2002).

[37] S. M. Wolfe, I. H. Hutchinson, R. S. Granetz, J. Rice, A. Hubbard, A. Lynn, P. Phillips, T. C. Hender, D. F. Howell, R. J. La Haye, and J. T. Scoville
Phys. Plasmas 12, 056110 (2005).

[38] J.L. Luxon, Nucl. Fusion **42** 614 (2002).

[39] C. Paz-Soldan, R.J. Buttery, A.M. Garofalo, J.M. Hanson, R.J. LaHaye, M.J. Lanctot, J.K. Park, W.M. Solomon and E.J. Strait, Nucl. Fusion 54 073013 (2014).

[40] P.B. Snyder, R.J. Groebner, J.W. Hughes, T.H. Osborne, M. Beurskens, A.W. Leonard, H.R. Wilson and X.Q. Xu, Nucl. Fusion **51**, 103016 (2011).

[41] Xi Chen, K.H. Burrell, T.H. Osborne, K. Barada, G.R. McKee, C.C. Petty, T.L. Rhodes, W.M. Solomon, T.M. Wilks, Z. Yan, T. Odstricil, D. Ernst, "Expanding the Parameter Space of the Wide-Pedestal QH-mode Towards ITER Conditions", submitted to Nuclear Fusion.

[42] T. S. Hahm and K. H. Burrell, Phys. Plasmas **2**, 1648 (1995).

[43] A. Pankin, D. McCune, R. Andre, G. Bateman, and A. H. Kritz, Comput. Phys. Commun. **159**, 157 (2004).

[44] W. M. Solomon, K. H. Burrell, A. M. Garofalo, S. M. Kaye, R. E. Bell, A. J. Cole, J. S. deGrassie, P. H. Diamond, T. S. Hahm, G. L. Jackson, M. J. Lanctot, C. C. Petty, H. Reimerdes, S. A. Sabbagh, E. J. Strait, T. Tala, and R. E. Waltz,
Phys. Plasmas **17**, 056108 (2010).

[45] C. Chrystal, K. H. Burrell, B. A. Grierson, S. R. Haskey, R. J. Groebner, D. H. Kaplan, and A. Briesemeister, Rev. Sci. Instrum. **87**, 11E512 (2016); doi: 10.1063/1.4958915

[46] S. R. Haskey, B. A. Grierson, L. Stagner, C. Chrystal, A. Ashourvan, A. Bortolon, M. D. Boyer, K. H. Burrell, C. Collins, R. J. Groebner, D. H. Kaplan, and N. A. Pablant, Rev. Sci. Instrum. **89**, 10D110 (2018); doi: 10.1063/1.5038349